Published in final edited form as:

IEEE Robot Autom Lett. 2016 ; 1(1): 98–105. doi:10.1109/LRA.2015.2507706.

Rapid, Reliable Shape Setting of Superelastic Nitinol for Prototyping Robots

Hunter B. Gilbert [Student Member, IEEE] and **Robert J. Webster III [Senior Member, IEEE]**

Department of Mechanical Engineering, Vanderbilt University, Nashville, TN 37235-1592 USA

Hunter B. Gilbert: hunter.b.gilbert@vanderbilt.edu; Robert J. Webster: robert.webster@vanderbilt.edu

Abstract

Shape setting Nitinol tubes and wires in a typical laboratory setting for use in superelastic robots is challenging. Obtaining samples that remain superelastic and exhibit desired precurvatures currently requires many iterations, which is time consuming and consumes a substantial amount of Nitinol. To provide a more accurate and reliable method of shape setting, in this paper we propose an electrical technique that uses Joule heating to attain the necessary shape setting temperatures. The resulting high power heating prevents unintended aging of the material and yields consistent and accurate results for the rapid creation of prototypes. We present a complete algorithm and system together with an experimental analysis of temperature regulation. We experimentally validate the approach on Nitinol tubes that are shape set into planar curves. We also demonstrate the feasibility of creating general space curves by shape setting a helical tube. The system demonstrates a mean absolute temperature error of 10°C.

Index Terms

Medical robots and systems; surgical robotics; steerable catheters/needles

I. Introduction

Nitinol alloys have long been used in robotics for their shape memory properties to produce motion as the temperature of the alloy is controlled [1]. The related superelastic property allows some Nitinol alloys to undergo large, reversible psuedo-elastic deformations at a constant temperature [2], and has enabled steerable needles [3], multi-backbone continuum robots [4], tendon-actuated continuum robots [5], and concentric tube robots [6]–[9], among others. It is sometimes useful in these robots (and more generally in medical devices [10]) to shape set a nonlinear space curve into the superelastic material. Indeed, for concentric tube robots in particular, this is what enables the robot to work at all.

In concentric tube robots, several precurved, superelastic Nitinol tubes are arranged concentrically. Each tube has a precurved shape, and when the tubes are axially rotated or translated the tubes must bend and twist one another in order to conform to a common centerline, which creates motion in the robot [7], [11]. Superelastic Nitinol is used because the high recoverable strain limit enables high pre-shaped curvatures in the individual tubes without plastic deformation, resulting in a larger robot workspace.

For concentric tube robots, the latest numerical design algorithms can produce specific tube precurvatures needed to accomplish surgical tasks such as intracerebral hemorrhage evacuation [12], transoral lung biopsy [13], intracardiac surgery [14], intraventricular interventions [15], transurethral prostate removal [16], and transnasal pituitary surgery [17]. Optimal design for stable robot operation has also been considered [18], [19]. In all of these cases, a set of tubes must be produced that matches the output of the design algorithm in order to test the results in a real prototype.

However, making curved devices out of Nitinol from the straight stock material one can typically purchase is not straightforward due to the difficulty of selecting the proper shape setting treatment that will both impart the desired shape accurately and retain the superelastic properties of the material. Optimization of the material properties of Nitinol is known to be a challenge [20], and creating optimized parts typically requires specialized equipment and considerable experience with specific techniques, which are often guarded as trade secrets. For Nitinol devices which are used clinically and produced in large quantities, the time and effort required to optimize the shape setting process is acceptable, but since custom fabrication of very low volume prototypes by Nitinol manufacturers introduces substantial costs and time delays into the research process, a quick, easy, and accurate shape setting technique is highly desirable for laboratory settings.

The creation of Nitinol samples with desired curvature and other properties (e.g. retaining superelasticity) typically requires many heat treatment attempts with different samples, varying treatment times and temperatures [21]. In general, many heating methods may be used, and the best have high heat transfer rates to the part and precise temperature control. Salt bath furnaces and fluidized beds are two of the best methods that have these properties, but the equipment required for these is expensive and potentially hazardous, making them poorly suited for quick prototyping in a typical laboratory setting. Hence, researchers are typically forced to resort to small box furnaces (ovens), despite the fact that shape setting is not highly repeatable or predictable using this method [22]. For concentric tube robots, shape setting in a box furnace has been described in the literature [9], [23].

In this paper, we propose an electrical shape setting technique, which is quick and easy to set up in a laboratory— particularly in academic laboratories focused on medical device or robotics prototyping rather than metallurgy. While this is not the first time electrical resistance heating of Nitinol has been proposed, and in fact commercial devices are available for shape setting orthodontic archwires [24], it is the first time that a practical, step-by-step method for electrical shape setting has been described for wires and tubes in the sizes and shapes commonly used in robotics. Smith and Hodgsen noted that electrical resistance annealing is one of many possible shape setting methods but did not provide details other than to note that care must be taken to avoid overheating [22]. Malard et al. presented results of high power electrical heat treatment of Nitinol wires but did not address re-shaping superelastic Nitinol, which is required in concentric tube robots and useful in prototyping other medical devices [25]. Using a commercially available electrical shape setting system for orthodontic archwires, Wang et al. showed that Joule heating for short times did not substantially alter the material properties, but longer heating times over 20 s did change the superelastic properties of the wires [24].

Our system uses real-time resistance measurements to regulate temperature, much like the resistance-based control techniques that have been explored in the area of shape-memory actuator control. Models for the solid state phase transition in electrically heated shape memory actuators have been developed to account for the interdependence of temperature, strain, and resistivity, and closed loop control of these actuators has been studied extensively using both resistance feedback and direct temperature feedback [26]–[30]. However, none of these papers address the use of superelastic Nitinol at room temperature, and moreover none address closed loop resistance feedback at the high temperatures needed to shape set Nitinol tubes and wires, where the change in resistivity is due to the natural temperature dependence of material resistivity rather than the phase transition.

The contribution of this paper is an inexpensive and easy to build electrical shape setting system with resistive feedback, together with practical insights for shape setting superelastic Nitinol parts accurately and repeatably in a typical robotics laboratory. Our approach is to heat superelastic Nitinol samples by pulsed direct current resistive heating. Through simultaneous power application and measurement, we show that it is possible to achieve rapid, reliable shape setting.

II. The Drawbacks of Box Furnace Shape Setting

Before describing the electrical shape setting approach that is the subject of this paper, we first motivate it by illustrating the challenges inherent to traditional furnace-based approaches. Furnace-based approaches are typically recommended by Nitinol manufacturers for low-volume prototyping applications in laboratories focused on medical device prototyping or robotics rather than metallurgical research.

Shape setting recommendations from Nitinol manufacturers include temperature ranges of 400–550 °C and time ranges from less than one minute to 20 minutes or more [31], [32]. The quality of results one obtains are highly sensitive to both the time and temperature used. Indeed, it is known that the specific time, temperature, fixture design and heating method will typically all need to be adjusted to obtain the desired results [21]. Thus, a large factorial study is typically required, which is feasible in commercial settings where high volumes are to be produced, but can be prohibitively time consuming and costly in low volume prototyping applications.

In a large factorial study of this type that lies within the recommended temperature and time ranges, many samples would emerge no longer superelastic, their transition temperatures having been accidentally moved above room temperature by the shape setting process. And even “successful samples” that remain superelastic and take on some curvature will often end up with curvatures substantially different than the desired curvature (i.e. the curvature of the jig into which they were placed).

To illustrate this by example, we followed exactly the time (10 minutes) and temperature (500 °C) recommended to us verbally by one manufacturer, which are also consistent with publicly available suggestions at manufacturers’ web sites [31], [32]. The process recommended by the manufacturer was:

1. Constrain the Nitinol in a metal fixture in the desired final shape.
2. Heat the part and fixture for 10 minutes in an air furnace at a temperature of 500 °C, and
3. Quench the part and fixture in room temperature water to sharply define the heating time and avoid aging effects.

We shape set a Nitinol tube according to this process in a fixture made from two aluminum plates with brass pins between them, which initially constrained the Nitinol to the desired curvature (see Fig. 1). The tube had an outer diameter of 1.16 mm and an inner diameter of 0.86 mm, and the fixture was designed with a radius of curvature of 33.3 mm.

As shown in Fig. 1, significant springback occurred when the part was removed from the fixture after shape setting. This effect makes the fabrication of a part with a desired shape difficult, since accounting for this much springback in the fixture would require additional experimentation, time and material.

Thus, shape setting Nitinol in a box furnace is challenging for low volume prototyping applications. To provide a better method of shape setting, we now turn our attention to the direct electrical internal heating method that is the subject of this paper.

III. Electrical Shape Setting

We use direct Joule heating to shape set Nitinol prototype parts. An electrical heating method is attractive, in particular, when the part to be shape set has one relatively long dimension and the electrical current can be made to pass through all the material which should be heated.

Electrical heating has several advantages over other heating methods. Probably the most important of these is the ability to rapidly heat the part to shape setting temperatures, which avoids aging effects. Furthermore, the equipment required for electrical heating is minimal, consisting of only a battery and the circuitry that controls the heating process. The applied voltage and current can also be easily monitored, making measurements of both the applied power and the part resistance readily available. We show in this section how to use the latter of these as a feedback signal to regulate the heating process and create a repeatable and accurate shape setting system.

A. Temperature Resistance Model

The temperature of the Nitinol sample can be inferred from measurement of the resistance, which is available during heating if the applied voltage and current are measured. Novák et al. reported an experimentally determined value of the linear austenitic temperature coefficient of resistivity for Nitinol of $\partial \rho_A / \partial T = 5 \times 10^{-2}$ μΩ-cm-°C^{-1}[33], which means that over a 500 °C temperature swing we expect a change in resistivity of 25 μΩ-*cm*. This represents a 25% increase over the nominal resistivity provided by the manufacturer of $\rho_A(T_{room}) = 100$ μΩ-*cm*, which is a measurable change in the part resistance that we use to infer the part temperature.

Assuming uniform heat transfer out of the part, we model the relative rise in the resistance of the part as a linear function of temperature $f(T) = \alpha T$, so that

$$\frac{R(T)}{R(T_{\text{room}})} - 1 = \alpha T. \quad (1)$$

After selecting a desired temperature T_d, the value $f(T_d)$ gives the relative rise in resistance, and $R(T)$ can then be controlled to achieve the desired value $R(T_d)$. Controlled application of the electrical power and accurate measurement of R enables the loop to be closed on a proxy for a temperature measurement.

B. Shape Setting System

A block diagram of our shape setting system is shown in Fig. 2, and a photograph of the physical circuit layout is provided in Fig. 3. Power is provided from a 12 V lead acid deep cycle battery (BCI Group Size 27), which is able to supply several kilowatts of instantaneous power during shape setting. An Arduino microcontroller board (μC), based on the Atmel ATmega328P processor, is programmed to cycle between an on-state and an off-state to regulate the measured resistance of the heated part. A MOSFET (International Rectifier, IRFB7430) controls the flow of current in response to commands from the μC. The MOSFET drain tab is mounted directly to a block of polished aluminum, which acts as both the conductive path and a heat sink. The MOSFET source is mounted to a second block of polished aluminum which is separated from the first block by an air gap. Welding cables carry current from the battery to the MOSFET mounting blocks, and also carry this current from the mounting blocks to the load, where spring-loaded clamps soldered to the end of the welding cable can be used to connect to short lengths of smaller gauge wire.

A gate driver (Texas Instruments, UCC37322P) provides high drive capability for the MOSFET gate, which allows the transistor to switch rapidly and prevents it from overheating. A 1 μF film capacitor and transient voltage suppression diode are placed across the MOSFET drain and source, in close proximity to the transistor, to snub inductive spikes, which result from the large di/dt values during switching. A flyback diode is also present near the MOSFET mounting blocks to provide a current path for the small parasitic inductance in the cables carrying current from the switch to the load. The voltage drop across the heated part is measured by a separate set of sense leads, which connect to a resistor voltage divider and difference amplifier (Texas Instruments, INA132). The current is measured by a 0.5 mΩ high-side shunt resistor and current monitor (Texas Instruments, INA139). The analog signals from the current and voltage monitor circuits are sampled by a 24-bit analog to digital converter (Texas Instruments, ADS1255), and the data is communicated to the μC via a serial peripheral interface (SPI) connection at 2 MHz.

C. Shape Setting Program

The μC program flow is graphically depicted in Fig. 4. The system is assumed to start with all parts at room temperature. The μC first closes the circuit and immediately thereafter measures the resistance of the part. Within each cycle of the μC code, the voltage and current

measurements are interleaved in rapid succession and the resistance is then calculated with the pair of measurements. This initial resistance measurement R_{init} is assumed to be at room temperature, and the target resistance R_t is selected as a function of the time t since the start command was given. The target resistance function $R_t(t)$ ramps linearly between the initial resistance and the final desired value $R_d = (1 + \alpha T_d)R_{init} = (\Delta R_d)R_{init}$, and is given by the equation

$$R_t(t) = \begin{cases} R_{\text{init}} + \frac{t}{t_{\text{ramp}}}(R_d - R_{\text{init}}) & t \leq t_{\text{ramp}} \\ R_d & t > t_{\text{ramp}} \end{cases} \quad (2)$$

The μC turns off the flow of current when $R(t) > R_t(t)$, and it resumes heating 100 ms after it turns off, repeating the cycle. While the heating circuit is turned on, resistance measurements are taken at a rate of 1 kHz. When the time t exceeds a total heating time defined by t_{ramp} and a second programmed interval t_{hold}, that is $t > t_{stop} = t_{ramp} + t_{hold}$, the system turns off and the part is left to cool without any additional quenching or forced cooling steps. Since the fixture is an insulator, the heating time is short, and the part has a low thermal mass, cooling occurs rapidly with natural convection.

IV. Fixture Design Guidelines

Due to the relatively low thermal mass of most of the parts that will be shape set, special care must be taken when designing the shape setting fixtures to promote uniform heating of the part. Both material selection and the jig shape are important in obtaining a successful shape setting. To minimize heat loss and promote uniform heating, the material for the fixture should have low thermal conductivity. Since the electrical path must not include the fixture, metallic jigs cannot be used. Ceramic materials are an option, but designing a custom fixture would involve substantial time spent machining the fixture. We have found that inexpensive medium density fiberboard (MDF) works well and can be fabricated into fixtures rapidly by laser cutting. It is electrically insulating and has a low thermal conductivity of about 0.25 W/m-K (compare to air at about 0.05 W/m-K at 700 K) [34]. This material does have an autoignition temperature (flame point) of about 245 °C, but we have never experienced a case in which the MDF has caught fire, in part due to a thin layer of charred material that forms at the hot surface of the MDF. Nevertheless, a fire extinguishing solution should be accessible when this type of jig is used.

One must also carefully design the fixture so that the heat transfer from the heated part to the fixture is nearly uniform. Ideally, this means that the fixture should be cut by computerized tools, such as a laser cutter, computer numerical controlled milling machine, or other precise means of manufacturing so that the slot which is cut to hold the part fully constrains its shape along the entire length. Non-uniform contact may cause localized overheating alternated with regions which do not attain a sufficiently high temperature to become shape set. If the fixtures are made from MDF, they should be replaced after one or two parts have been shape set due to material removal which occurs at the charred surface of the jig.

Additionally, the electrical connections to the part should be either accommodated within the length of the fixture or placed immediately where the part exits the ends of the fixture, because any length of the part which is heated by current and is surrounded only by air may overheat. Conversely, the wires for power delivery and sensing are heat sinks, and lower temperatures are attained in close proximity to these connections. In practice, this means that parts may be less precisely shaped near the ends of the fixture. In many cases, this discrepancy can be accounted for in the design of the fixture. For example, to curve only the end of an otherwise straight part, straight lengths of about a centimeter may be added to either end of the curved portion of the fixture. The part can be trimmed to length after shape setting to produce a curve at the end of the tube or wire. Another option is to increase the jig curvature near the ends to compensate for any loss in curvature.

For planar parts, we recommend a jig which is split along the axial length of the part like the one in Fig. 5 and can be clamped onto the part to hold it in place. Clamping pressure should be high enough to prevent movement of the part, but excessive pressure results in increased charring of the jig and the possibility of crushing tubular parts. In our experience, these types of jigs result in sufficiently uniform heating, and they have the advantage that they can be fabricated and set up quickly.

V. System Performance

To evaluate the performance of the shape setting system, we have studied both the accuracy of the temperature regulation and the ability of the system to produce the desired final results. We will first present measurements of the part temperatures achieved by the system, and then show several case studies of parts that we have created with this method.

A. Thermal Regulation

To obtain temperature measurements, a type K thermocouple of 0.01 in diameter was used to measure the actual temperature of a Nitinol tube suspended in the air as it was heated by the system. A photograph of the experimental setup is shown in Fig. 6. The thermocouple wire was wrapped around the tube with the junction located against the tube. The temperature measurement was taken with an Amprobe AM-270 multimeter, which was set to record the maximum value, and for each chosen test point ΔR_d, the maximum temperature measured during the heating process was recorded.

Tests were performed on a single Nitinol tube with an outer diameter of 2.18 mm and an inner diameter of 2.02 mm. The length of tubing between the power leads was 7 cm. The manufacturer’s material data sheet indicated the material is fully superelastic above 7.8 °C. The tube was supported at both ends and 18 gauge wires were tied in an overhand knot around the tube at each end. The knots were filled with 60/40 Sn/Pb solder to improve contact (note that this kind of solder does not wet to Nitinol, but the increased surface area improves electrical contact). The two voltage sensing clips were placed on the tube outside the supports, while the power wires were attached inside the supports to avoiding heating in the support regions where large contact areas are present.

The test points ΔR_d were chosen as 40 values ranging between 1.15 and 1.23, with the order chosen randomly. The selected target resistance was programmed into the shape setting program of Section III-C, with the parameters t_{ramp} = 3 s and t_{hold} = 30 s. At least five minutes were provided for the system to cool to room temperature in between trials. Room temperature during the trials ranged between 20–22 °C, and was manually recorded immediately prior to the collection of each data point.

B. Thermal Regulation Results

Fig. 7 shows that the increase in part temperature and the chosen value of ΔR_d correlate strongly (R^2 = 0.97). The best linear fit, when constrained to pass through the origin of the graph, has slope 1/α = 2438 °C. Two outliers (not shown in the figure) were removed from the data before fitting. These outliers were the first two measurements, which were taken before the formation of a sufficient oxide layer on the surface of the tube to prevent electrical conduction from the tube to the bare thermocouple wire. The results of the experiment indicate that a relative increase in resistance may be used as a proxy for temperature measurement. The maximum absolute error between the temperature data and the best fit line is 29 °C, and the mean absolute error is 10 °C. 89% of the measurements fall within 20 °C of the best fit line.

Over the course of the trials, the initial resistance reading of the part varied between 116.2 mΩ at the first trial to 112.9 mΩ at the last trial. The average initial resistance reading across all 40 trials was 112.7 mΩ, with standard deviation 0.7 mΩ. This illustrates that the initial part resistance at room temperature is predictable despite the varying thermal treatment history across the trials.

Although the purpose of this experiment is not to accurately determine the material properties of Nitinol, it is possible to compare the linear fit to the temperature coefficient of resistivity of Nitinol provided by Novák et al. [33]. Using that coefficient, we estimate

$$\frac{1}{\alpha}=\frac{100\mu\Omega-\mathrm{cm}}{5\times10^{-2}\mu\Omega-\mathrm{cm}-^{\circ}\mathrm{C}^{-1}}=2000^{\circ}\mathrm{C}, \quad (3)$$

by assuming a nominal room temperature resistivity of austenitic Nitinol of 100 μΩ-cm, as quoted by manufacturers [31]. Considering the slight nonuniformity of heating caused by the heat sinking effect of the power leads, this comparison indicates that the shape setting system is operating correctly. We also note that if the linear fit is not constrained to pass through the origin, the slope of the best fit line becomes 1/α = 2089 °C.

C. Repeatability Assessment

To assess the repeatability of this shape setting method, we shape set 10 wires into a 90 degree arc, with a target radius of curvature of r_{jig} = 63.7 mm and a curved length of 100 mm. Each wire was placed in a split fixture of the same type shown in Fig. 5, except that the solder-filled knots were replaced with standard laboratory test clip leads for their ease of use. The wire was first heated using parameters ΔR_d = 1.15, t_{ramp} = 5 s, and t_{heat} = 15 s. After cooling for at least two minutes, it was heated again with ΔR_d = 1.21 and the same

time parameters. If after removing the wire from the fixture significant springback was observed, it was heated for a third time at $\Delta R_d = 1.21$ with the same time parameters. The wires were then scanned using a flatbed scanner at 600 dpi and the angle between the tangents at the wire ends measured. This angle measurement was then converted to a radius of curvature using the curved jig length.

The mean radius of curvature of the resulting wires was 65.1 mm and the standard deviation was 1.7 mm. Maximum and minimum radii of curvature were 68.1 mm and 62.6 mm, respectively. We note that two of the wires in the trial required a third heating, with the remaining eight only requiring two heating cycles. We strongly suspect that the reason for requiring the third heating was due to imperfect electrical contact made by the test clip leads in the voltage sensing circuit.

D. Planar Tube Examples

Fig. 8 shows multiple Nitinol tubes that were successfully shape set using this method. For each tube, the heating method and parameters of Section III-B was used without modification. Each tube was placed into an MDF jig similar to the one of Fig. 5 and heated twice. The jigs were designed to impart a constant radius of curvature to the centerline of the tube over an arc length ranging from 42–52 mm. The radii of curvature ranged from 130 mm to 60 mm. In a first heating cycle a desired resistance increase $\Delta R_d = 1.15$ was used, and in a second heating cycle, after the system was allowed to cool to room temperature, the desired resistance increase was set to $\Delta R_d = 1.21$. In both heating cycles, the timing parameters were $t_{ramp} = 3$ s and $t_{hold} = 7$ s.

Table I shows the results for the three tubes in Fig. 8 and the results for the two tubes which were compared in Fig. 1. The value r_{jig} describes the radius of curvature of the arc as designed into the fixture, and the value r_{tube} describes the radius of curvature of the tube after shape setting.

E. Helical Tube Example

To explore whether we could shape set a non-planar curve, we performed another experiment in which we sought to make a helical specimen. The tube had a 1.14 mm outer diameter and 0.97 mm inner diameter. The fixture was prepared by slicing (in a CAD program) the cylindrical solid model shown in Fig. 9 into thin axial slices 0.85 mm thick, and each of these was then laser cut from Birch plywood of the same thickness. The square shaft shown in the figure holds the slices in the correct orientation so that the shape is retained when the slices are assembled into the fixture and the wire inserted. This helix was created for an MRI compatible robot application involving thermal treatment for epilepsy in the brain (see [35] for further information).

F. Discussion

Repeated heating cycles were employed in the above examples. In many cases it is advantageous to repeat the program more than once for a single part, with increasing values of ΔR_d. This repetition mitigates the effects of stress recovery, which slightly lowers material resistivity during shape setting. It also mitigates the effect of the phase transition

which occurs in any areas which have transformed from Austenite to Martensite under the applied stress of the fixture. These regions transform back to Austenite upon heating, which causes an increase in resistivity. By performing two or three cycles and slowly increasing ΔR_d, overheating and underheating can both be avoided.

VI. Conclusions

In conclusion, we have presented a complete system for closed loop, high temperature resistance heating of Nitinol and design guidelines for fixtures that can be used with this system. The system produces rapid and reliable results, which is particularly useful for low volume laboratory prototyping applications. For concentric tube robots, this system will facilitate accurate fabrication to implement the results of emerging numerical optimal design results for many potential surgical applications. We also believe it will be generally useful for medical device prototyping laboratories and robotics laboratories that wish to shape set superelastic Nitinol for a wide variety of current and future applications.

Acknowledgments

This work was supported in part by the National Science Foundation (NSF) under Grant iis-1054331 and Graduate Research Fellowship dge-0909667 and in part by the National Institutes of Health (NIH) under Grants R01-eb017467 and R21-ns087796. The content is solely the responsibility of the authors and does not necessarily represent the official views of the National Science Foundation or the National Institutes of Health.

References

1. Jani JM, Leary M, Subic A, Gibson MA. a review of shape memory alloy research, applications and opportunities. Mater. Des. 2014; 56:1078–1113.
2. Duerig T, Pelton A, Stöckel D. An overview of Nitinol medical applications. Mater. Sci. Eng. A. 1999 Dec.273–275:149–160.
3. Reed KB, et al. Robot-assisted needle steering. Robot. Autom. Mag. 2011; 18(4):35–46.
4. Ding J, Goldman R, Xu k, Allen P, Fowler D, Simaan N. Design and coordination kinematics of an insertable robotic effectors platform for single-port access surgery. IEEE/ASME Trans. Mechatron. 2013 Oct; 18(5):1612–1624.
5. Murphy RJ, Kutzer MDM, Segreti SM, Lucas BC, Armand M. Design and kinematic characterization of a surgical manipulator with a focus on treating osteolysis. Robotica. 2014; 32(6): 835–850.
6. Gilbert, HB.; Webster, RJ. Concentric tube robots: state of the art and future directions. In: Inaba, M.; Corke, P., editors. Robotics Research: The 16th International Symposium ISRR (Springer Tracts in Advanced Robotics). Vol. 114. New York, NY, USA: Springer; 2016.
7. Dupont PE, Lock J, Itkowitz B, Butler E. Design and control of concentric-tube robots. IEEE Trans. Robot. 2010 Apr; 26(2):209–225. [PubMed: 21258648]
8. Rucker DC, Jones BA, Webster RJ III. A geometrically exact model for externally loaded concentric tube continuum robots. IEEE Trans. Robot. 2010 Oct; 26(5):769–780. [PubMed: 21566688]
9. Torabi M, Gupta R, Walsh CJ. Compact robotically steer-able image-guided instrument for multi-adjacent-point (MAP) targeting. IEEE Trans. Robot. 2014 Aug; 30(4):802–815.
10. Poncet PP. Nitinol medical device design considerations. Proc. Int. Conf. Shape Memory Superelastic Technol. 2000; 2(4):441–455.
11. Webster RJ III, Romano JM, Cowan NJ. Mechanics of precurved-tube continuum robots. IEEE Trans. Robot. 2009 Feb; 25(1):67–78.
12. Burgner J, Swaney PJ, Lathrop RA, Weaver KD, Webster RJ III. Debulking from within: A robotic steerable cannula for intracerebral hemorrhage evacuation. IEEE Trans. Biomed. Eng. 2013 Sep; 60(9):2567–2575. [PubMed: 23649131]

13. Swaney, PJ., et al. Tendons, concentric tubes, and a bevel tip: Three steerable robots in one transoral lung access system; Proc. IEEE Int. Conf. Robot. Autom; 2015. p. 5378-5383.
14. Bedell, C.; Gosline, A.; Dupont, PE. Design optimization of concentric tube robots based on task and anatomical constraints; Proc. IEEE Int. Conf. Robot. Autom; 2011. p. 398-403.
15. Bergeles C, Gosline AH, Vasilyev NV, Codd PJ, del Nido PJ, Dupont PE. Concentric tube robot design and optimization based on task and anatomical constraints. IEEE Trans. Robot. 2015 Feb; 31(1):67–84. [PubMed: 26380575]
16. Hendrick, RJ.; Herrell, SD., III; Webster, RJ. A multi-arm handheld robotic system for transurethral laser prostate surgery; Proc. IEEE Int. Conf. Robot. Autom; 2014. p. 2850-2855.
17. Burgner J, et al. A telerobotic system for transnasal surgery. IEEE/ASME Trans. Mechatron. 2014 Jun; 19(3):996–1006.
18. Ha, J.; Park, FC.; Dupont, PE. Achieving elastic stability of concentric tube robots through optimization of tube precurvature; Proc. IEEE/RSJ Int. Conf. Intell. Robots Syst; 2014. p. 864-870.
19. Hendrick, RJ.; Gilbert, HB.; Webster, RJ, III. Designing snap-free concentric tube robots: A local bifurcation approach; Proc. IEEE Int. Conf. Robot. Autom; 2015. p. 2256-2263.
20. Pelton AR, Dicello J, Miyazaki S. Optimisation of processing and properties of medical grade Nitinol wire. Minimally Invasive Therapy Allied Technol. 2000 Jan; 9(2):107–118.
21. Morgan, NB.; Broadley, M. Taking the art out of smart!—Forming processes and durability issues for the application of NiTi shape memory alloys in medical devices; Proc. Med. Device Mater. Mater. Processes Med. Devices Conf; 2003. p. 247-252.
22. Smith, SA.; Hodgson, DE. Shape setting Nitinol; Proc. Med. Device Mater. Mater. Processes Med. Devices Conf; 2003. p. 266-270.
23. Kim, J-S.; Lee, D-Y.; Kim, K.; Kang, S.; Cho, K-J. Toward a solution to the snapping problem in a concentric-tube continuum robot: Grooved tubes with anisotropy; Proc. IEEE Int. Conf. Robot. Autom; 2014. p. 5871-5876.
24. Wang YB, Zheng YF, Liu Y. Effect of short-time direct current heating on phase transformation and superelasticity of Ti-50.8at.%Ni alloy. J. Alloys Compd. 2009; 477:764–767.
25. Malard B, Pilch J, Sittner P, Gartnerova V, Grenoble H. Microstructure and functional property changes in thin Ni-Ti wires heat treated by electric current—High energy X-ray and TEM investigations. Funct. Mater. Lett. 2009; 2(2):45–54.
26. Ikuta, K.; Tsukamoto, M.; Hirose, S. Shape memory alloy servo actuator system with electric resistance feedback and application for active endoscope; Proc. IEEE Int. Conf. Robot. Autom; 1988. p. 427-430.
27. Song G, Chaudhry V, Batur C. Precision tracking control of shape memory alloy actuators using neural networks and a sliding-mode based robust controller. Smart Mater. Struct. 2003; 12(2):223–231.
28. Ma N, Song G, Lee HJ. Position control of shape memory alloy actuators with internal electrical resistance feedback using neural networks. Smart Mater. Struct. 2004; 13(4):777–783.
29. Dutta SM, Ghorbel FH. Differential hysteresis modeling of a shape memory alloy wire actuator. IEEE/ASME Trans. Mechatron. 2005 Apr; 10(2):189–197.
30. Ho M, McMillan AB, Simar JM, Gullapalli R, Desai JP. Toward a meso-scale SMA-actuated MRI-compatible neurosurgical robot. IEEE Trans. Robot. 2012 Feb; 28(1):213–222.
31. Johnson Medical Components. [accessed on Apr. 8, 2015] Nitinol Shape Setting [Online]. Available: http://jmmedical.com/resources/251/Nitinol-Shape-Setting.html
32. Nitinol Devices & Components, Inc. [accessed on Apr. 8, 2015] Nitinol Facts [Online]. Available: http://www.nitinol.com/nitinol-university/nitinol-facts
33. Novák V, Šittner P, Dayananda G, Braz-Fernandes F, Mahesh K. Electric resistance variation of NiTi shape memory alloy wires in thermomechanical tests: Experiments and simulation. Mater. Sci. Eng. A. 2008 May.481–482:127–133.
34. Zhou J, Zhou H, Hu C, Hu S. Measurements of thermal and dielectric properties of medium density fiberboard with different moisture contents. BioResources. 2013; 8(3):4185–4192.

35. Comber DB, Barth EJ, Webster RJ III. Design and control of an magnetic resonance compatible precision pneumatic active cannula robot. ASME J. Med. Devices. 2014; 8(1):011003.

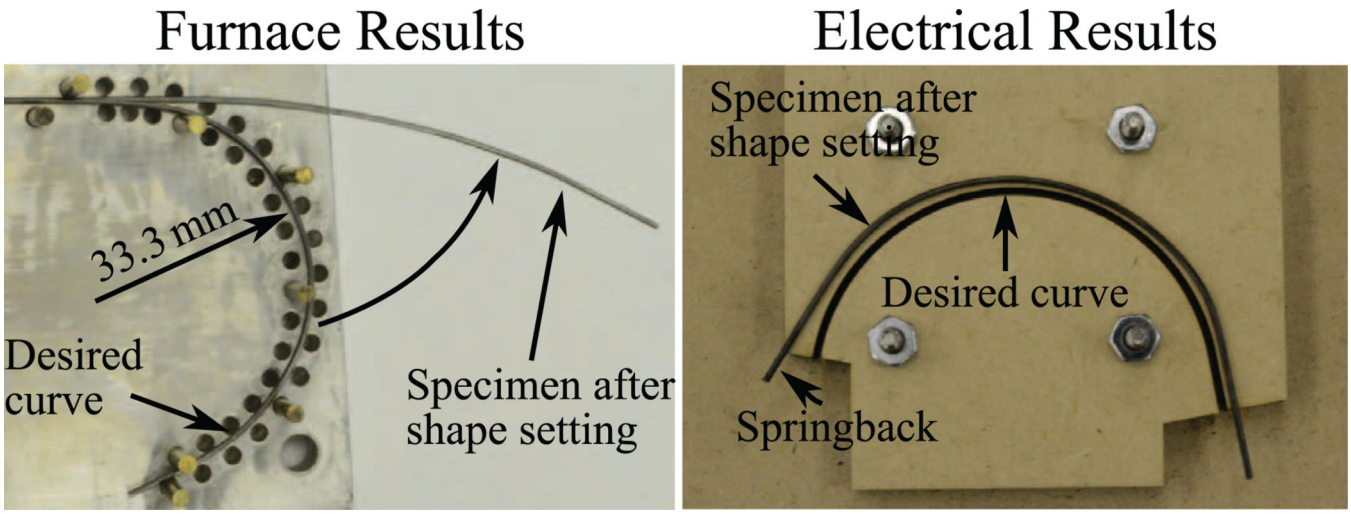

Fig. 1.

A comparison of traditional air furnace-based shape setting and the electrical technique we describe in this paper. (Left) A fixture with metal pins was placed in the oven at manufacturer recommended temperature and duration. The sample does take on precurvature, but with a much lower curvature than the desired 33.3 mm radius (i.e. with substantial springback). (Right) The electrical shape setting approach we present in this paper produces much more accurate results with less springback.

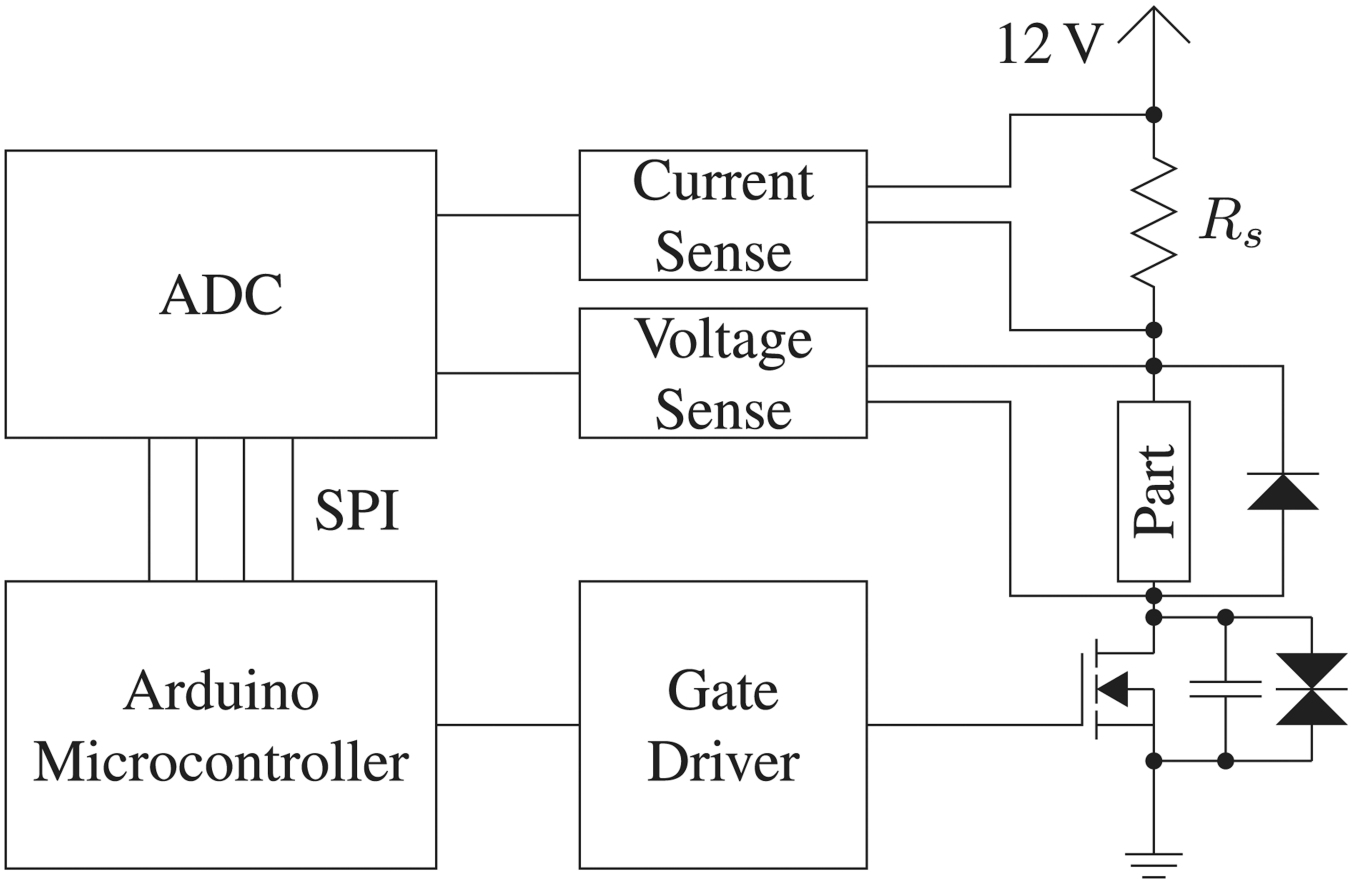

Fig. 2.

Block diagram of the system structure. The microcontroller controls the part resistance by measuring it while power is flowing through the part. The capacitor and TVS diode across the MOSFET, as well as the flyback diode across the part, protect the system from the inductive voltage spike caused at turn-off.

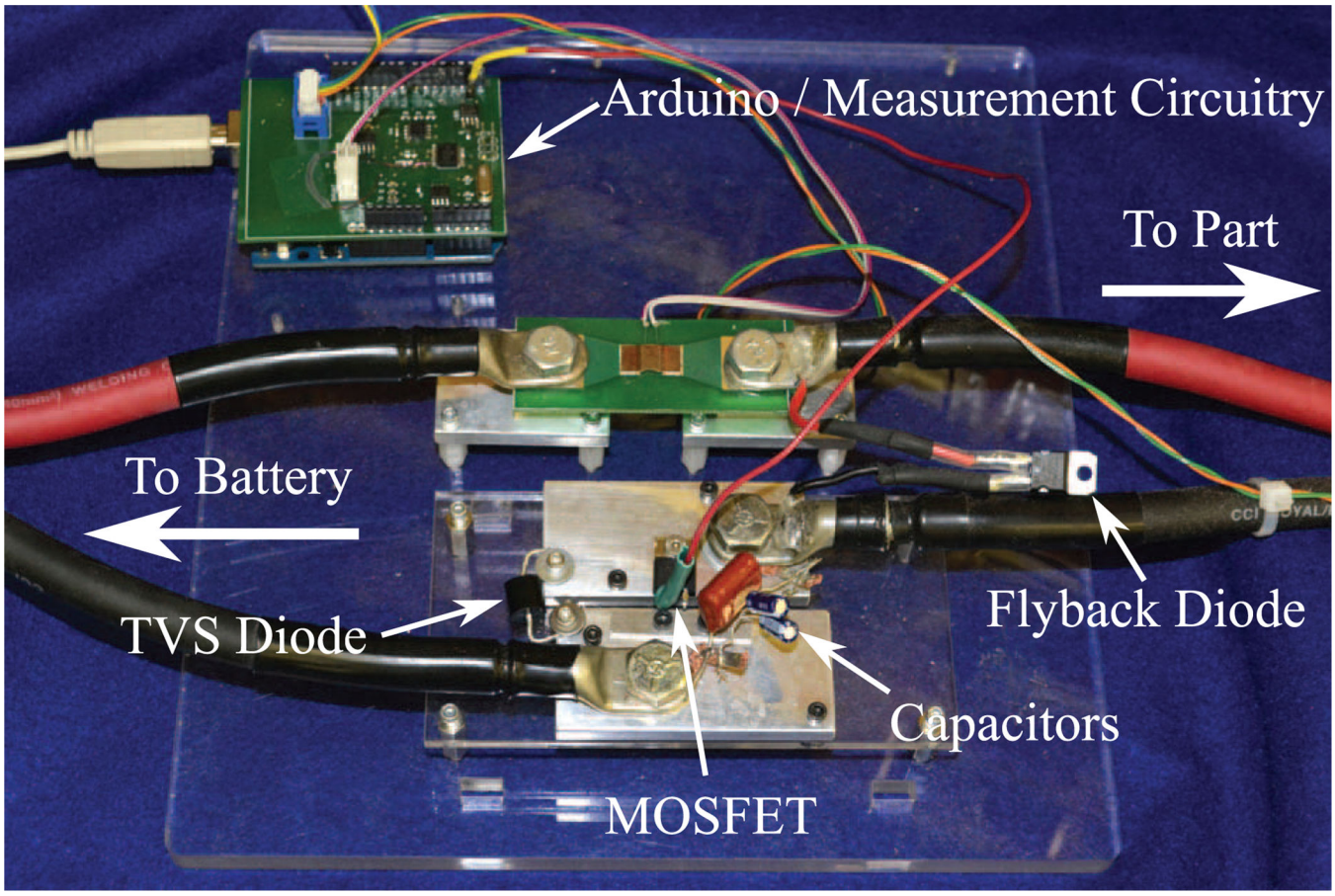

Fig. 3.
Photograph of the circuit layout. The lower aluminum blocks are mounting points for the MOSFET, and the upper aluminum blocks are mounting locations for the sense resistor.

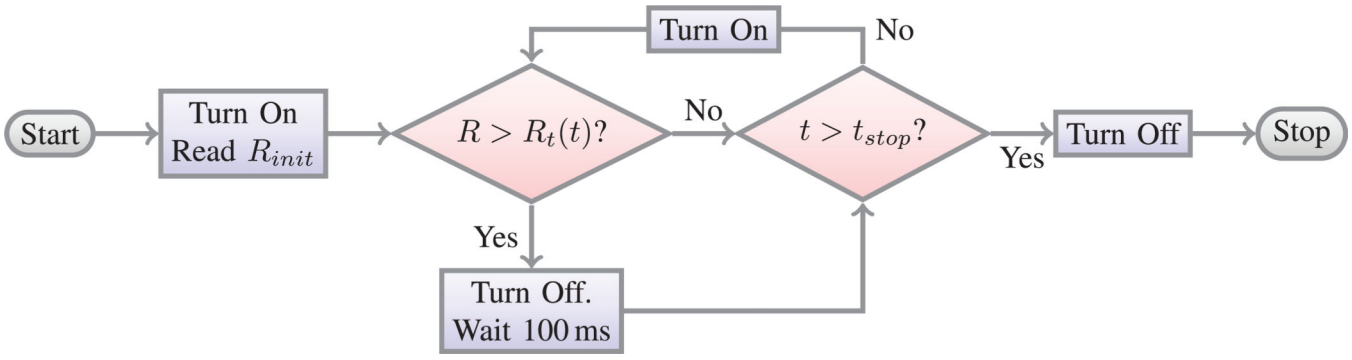

Fig. 4.

A flow chart of the μC program which controls the heating of the part. The inner loop runs at a rate such that the resistance check occurs every 1 ms when the power is turned on. At the start condition $t = 0$, and the value $t_{stop} = t_{ramp} + t_{hold}$.

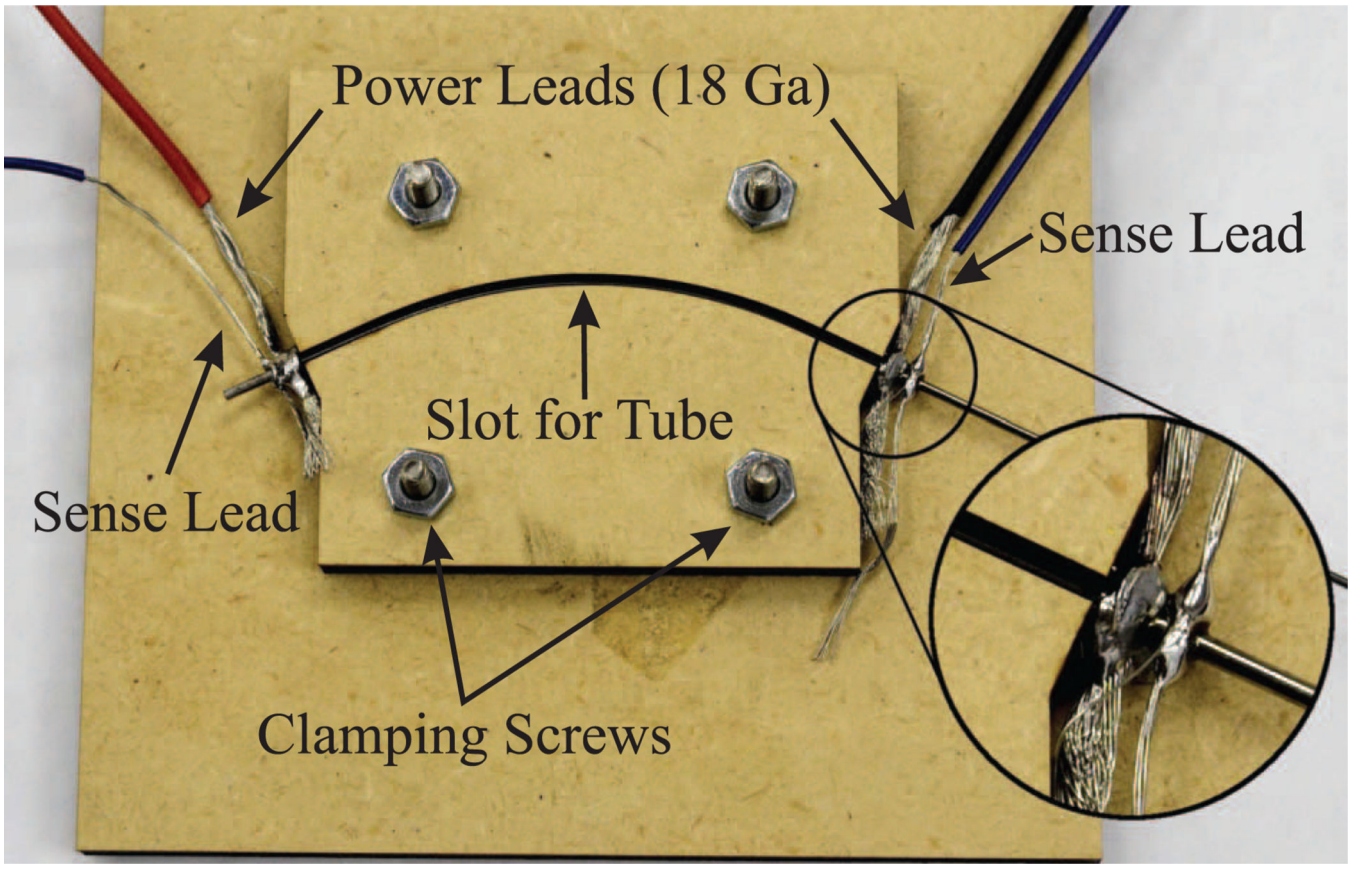

Fig. 5.

This fixture made of MDF was cut by a CNC laser cutter. The slot for the part is made to accommodate the diameter of the tube which it was designed for, accounting for the kerf width of the laser cutter. Wires are tied in an overhand knot and filled with solder to improve electrical contact.

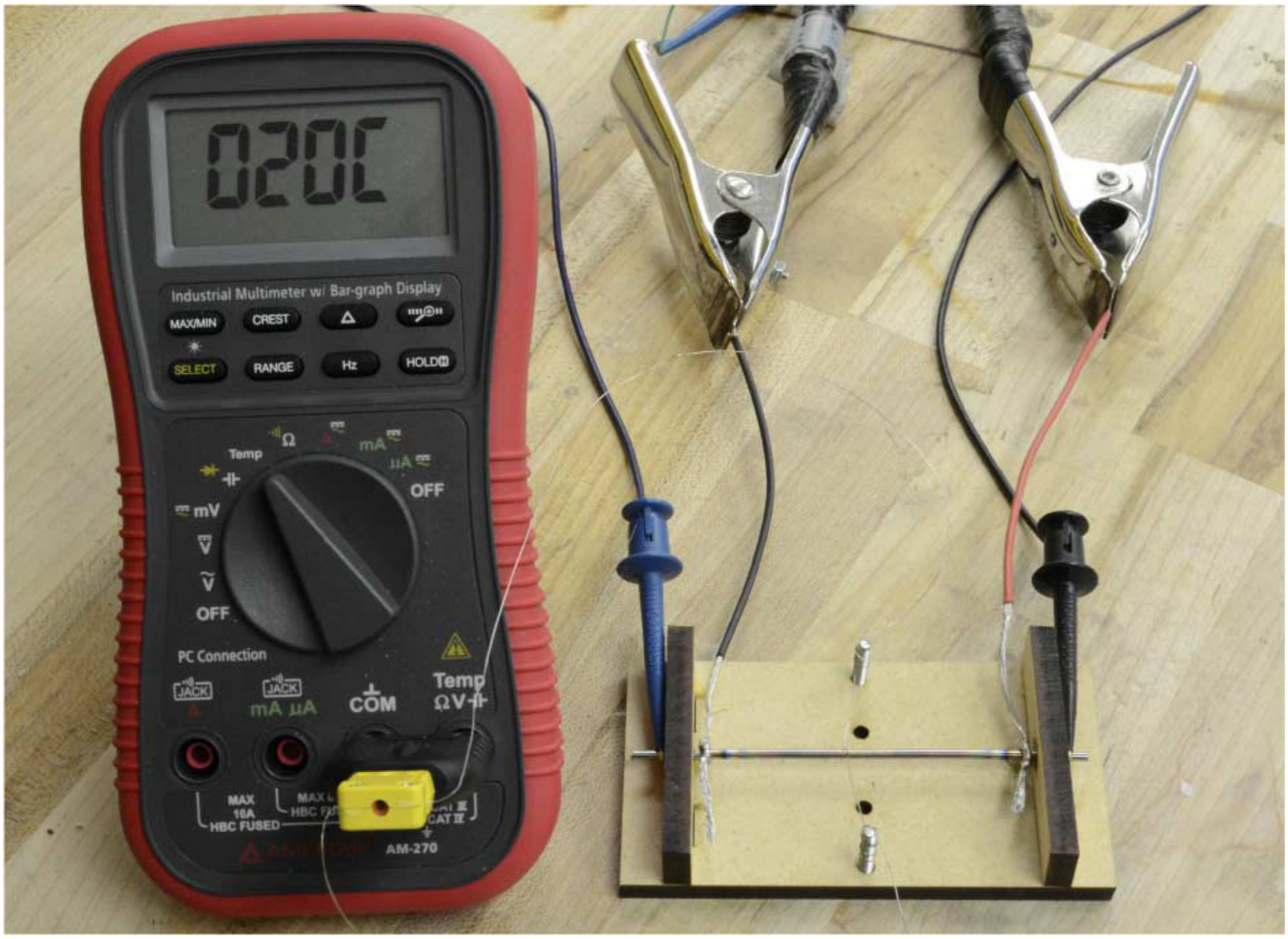

Fig. 6.
The experimental setup for collecting temperature data.

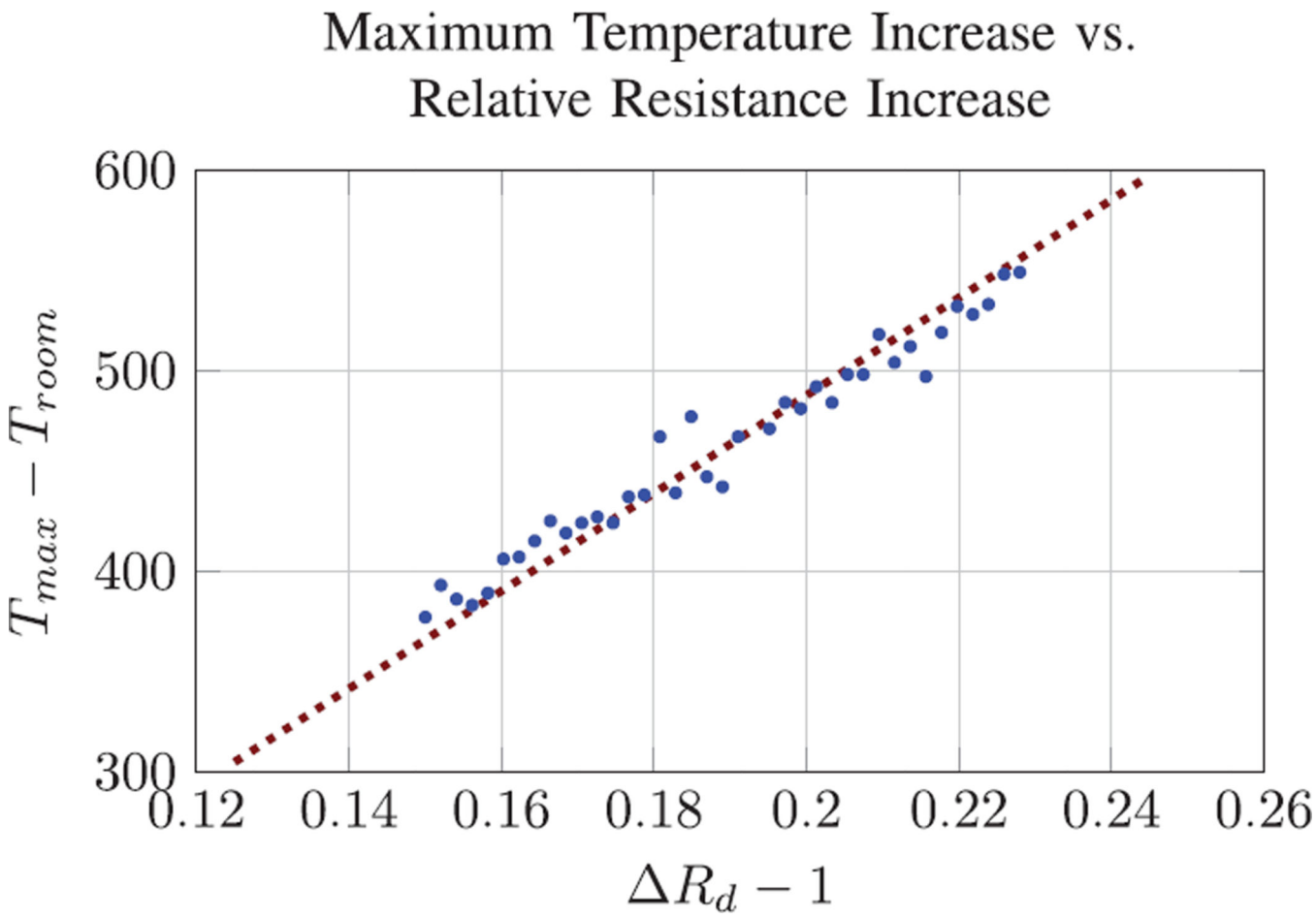

Fig. 7.

The correlation between temperature increase and target relative resistance increase. The coefficient of the best fit line, constrained to pass through origin, is $1/\alpha$ = 2438°C.

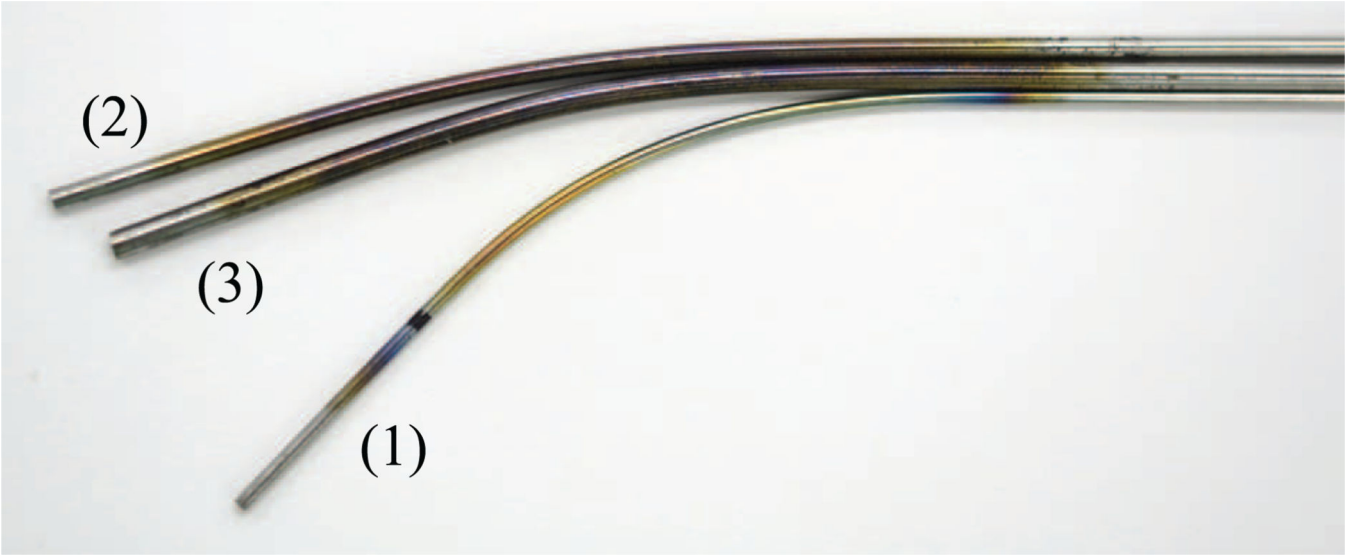

Fig. 8.

Multiple Nitinol tubes of varying diameters that have been shape set to different curvatures. This photograph was taken immediately after shape setting of each tube, before any additional cleaning or trimming operations. The coloration of the tubes in the heated region is a result of surface oxidation and fixture charring.

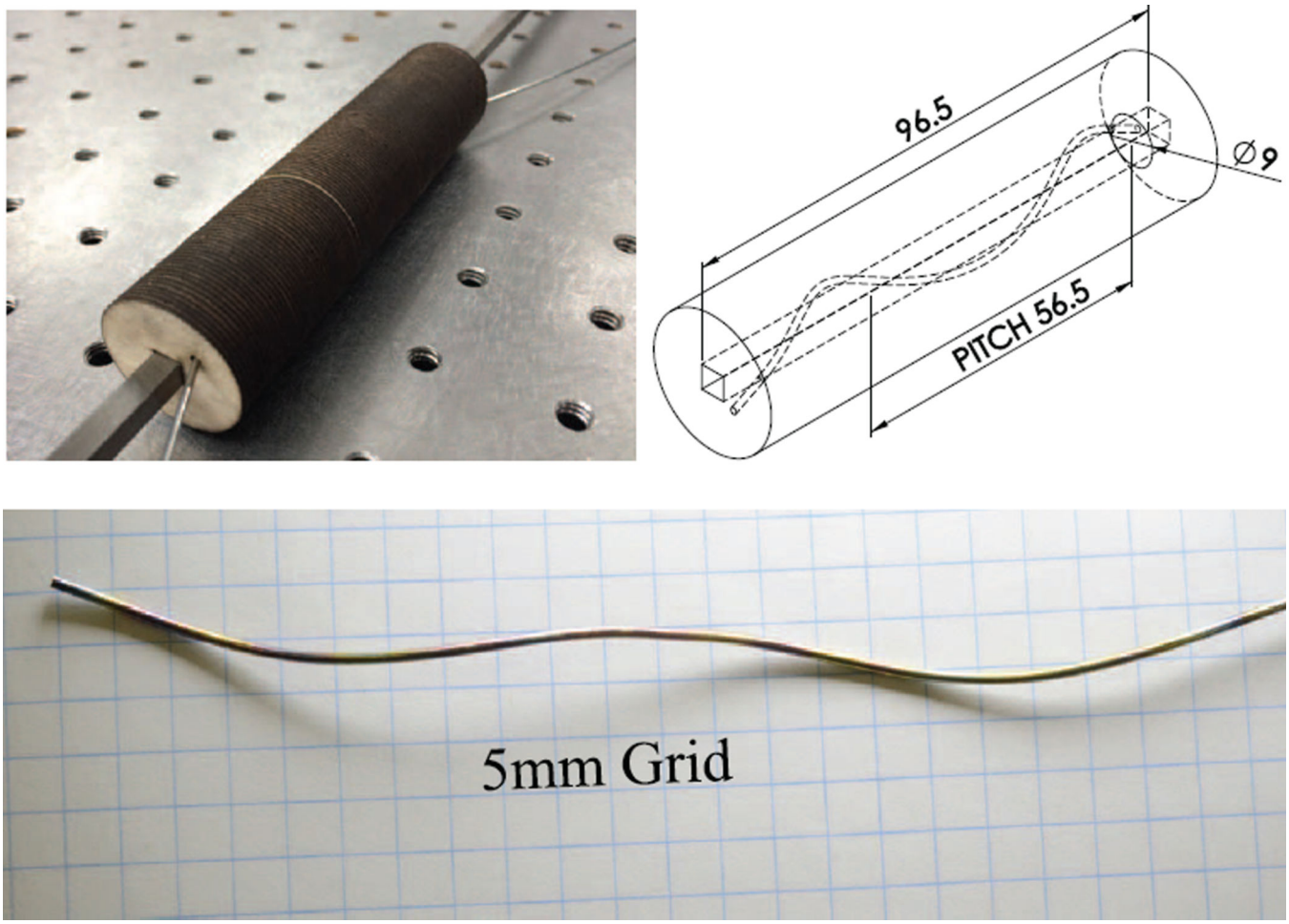

Fig. 9.

(Top Left) This jig for a helical tube was formed by slicing the fixture into discrete cross sections. Each cross section is made of a 0.85 mm thick sheet of birch plywood. (Top Right) Dimensions of the helix that the tube was constrained to. (Bottom) The tube is shown after shape setting.

TABLE I

The Tube Dimensions, and Radii of Curvature of the Jigs and Shape Set Tubes. All Values Have Units of mm

Tube	OD	ID	r_{jig}	r_{tube}
Fig. 8(1)	1.16	0.86	59.5	64.5
Fig. 8(2)	1.92	1.57	129.9	144.8
Fig. 8(3)	2.48	2.25	107.5	121.7
Fig. 1 (Furnace)	1.16	0.86	33.3	169.9
Fig. 1 (Electrical)	1.16	0.86	33.3	36.6